

This discussion paper is/has been under review for the journal Biogeosciences (BG).
Please refer to the corresponding final paper in BG if available.

Evaluating the ocean biogeochemical components of earth system models using atmospheric potential oxygen (APO) and ocean color data

C. D. Nevison¹, M. Manizza², R. F. Keeling², M. Kahru², L. Bopp³, J. Dunne⁴,
J. Tjiputra⁵, and B. G. Mitchell²

¹University of Colorado, Boulder, Institute for Arctic and Alpine Research, Boulder, Colorado, USA

²Scripps Institution of Oceanography, La Jolla, California, USA

³IPSL/LSCE, UMR8212, CNRS-CEA-UVSQ, Gif sur Yvette, France

⁴National Oceanic and Atmospheric Administration/Geophysical Fluid Dynamics Laboratory, Princeton, New Jersey, USA

⁵Uni Climate, Uni Research and Bjerknes Centre for Climate Research, Allegaten 70, 5007 Bergen, Norway

8485

Received: 1 April 2014 – Accepted: 3 May 2014 – Published: 11 June 2014

Correspondence to: C. D. Nevison (cynthia.nevison@colorado.edu)

Published by Copernicus Publications on behalf of the European Geosciences Union.

8486

Abstract

The observed seasonal cycles in atmospheric potential oxygen (APO) at a range of mid to high latitude surface monitoring sites are compared to those inferred from the output of 6 Earth System Models participating in the fifth phase of the Coupled Model Inter-comparison Project (CMIP5). The simulated air–sea O_2 fluxes are translated into APO seasonal cycles using a matrix method that takes into account atmospheric transport model (ATM) uncertainty among 13 different ATMs. Half of the ocean biogeochemistry models tested are able to reproduce the observed APO cycles at most sites, to within the current large ATM uncertainty, while the other half generally are not. Net Primary Production (NPP) and net community production (NCP), as estimated from satellite ocean color data, provide additional constraints, albeit more with respect to the seasonal phasing of ocean model productivity than the overall magnitude. The present analysis suggests that, of the tested ocean biogeochemistry models, CESM and GFDL ESM2M are best able to capture the observed APO seasonal cycle at both Northern and Southern Hemisphere sites. In the northern oceans, the comparison to observed APO suggests that most models tend to underestimate NPP ~~or~~ deep ventilation or both.

1 Introduction

Ocean physical and biogeochemical processes have profound influences on Earth's climate. Phytoplankton in the sunlit part of the ocean convert carbon from inorganic to organic form via photosynthesis, thereby establishing the base of the ocean food chain. Primary production and subsequent export of organic carbon from the mixed layer (export production) and remineralization at depth are key components of the so-called “biological pump,” which regulates the partition of carbon between the ocean and atmosphere (Gruber and Sarmiento, 2002; Boyd and Doney, 2003).

8487

Export production (EP) and the related process of net community production (NCP) are also important for understanding the distribution of dissolved O_2 within the ocean and the flux of O_2 (F_{O_2}) at the air–sea interface. NCP is defined here as the net amount of organic carbon fixed through photosynthesis over the depth of the mixed layer after accounting for grazing and both autotrophic and heterotrophic respiration. NCP is closely linked to F_{O_2} , since each mole of photosynthetically fixed carbon that persists beyond the time scale of air–sea exchange (2–3 weeks) leaves a stoichiometric amount of O_2 available for release to the atmosphere (Keeling et al., 1993). Release of O_2 to the atmosphere in association with NCP occurs mainly in the spring and summer at extratropical latitudes (Manizza et al., 2012). EP more or less balances NCP when averaged over a full year or if the upper ocean is in a long-term steady state (Laws et al., 2000). The exported carbon subsequently is respired in the subsurface ocean, leading to O_2 depletion at depth, which is replenished by both NCP in spring and summer and absorption from the atmosphere when the deep waters mix back to the surface in fall and winter. Deep ventilation and NCP thus are distinct processes that are largely separate in time and space but are both closely linked to the biological pump critical for ocean uptake of atmospheric CO_2 .

To explore the impacts of future climate change on Earth's climate and ecosystems, the Coupled Model Intercomparison Project phase 5 (CMIP5) relies on 3-dimensional numerical Earth System Models (ESMs), which incorporate descriptions of biogeochemical impacts of land and marine biota. Projections of future atmospheric CO_2 levels and associated climate warming in CMIP5 depend not only on fossil fuel use projections but also on assumptions about uptake and storage of carbon by the land and ocean. The oceans have absorbed approximately one third of the anthropogenic carbon released to the atmosphere since the beginning of the industrial era (Khatiwala et al., 2009), but this fractional rate of uptake is unlikely to continue in the future as the buffering capacity of surface waters declines and the export of carbon from the surface to the deep ocean fails to keep pace with anthropogenic fossil fuel combustion (Arora et al., 2013). Changes in ventilation of abyssal deepwater are an additional possible

NCP should come first, with EP being the related process"

The first sentence need to be clarified as to if it C or O2 that is "replenished" ? And the second here also needs to clarify the links to biological pump.

8488

consequence of future climate forcing that current models may or may not be able to predict accurately (Sigman et al., 2010).

Recent studies have tested the present-day skill of the ocean components of ESMs and some have also examined future projections (Schneider et al., 2008; Steinacher et al., 2010; Bopp et al., 2013; Anav et al., 2013). These evaluations have compared model output to both hydrographic measurements and remotely sensed ocean color products, most commonly net primary production (NPP). The models predict spatial-annual patterns in NPP that reproduce some of the main features seen in satellite data, but differ by over a factor of 2 in NPP magnitude. Some evaluations have examined seasonal variability and have found that ocean models tend to underestimate observed NPP at high latitudes (poleward of 44°) in the Northern Hemisphere and overestimate it in the Southern Hemisphere. The models also fail to capture the timing of the observed high latitude peak in NPP in both hemispheres, with predictions that are often 1–2 months earlier than observations (Anav et al., 2013; Henson et al., 2013). However, ocean color-derived NPP values are uncertain, especially in the Southern Ocean, reducing confidence in the “observed” constraints.

Many biogeochemical processes that are expected to occur in the future, such as responses to warming and stratification, are also highly relevant on seasonal time scales. Thus, challenging models against known seasonal variations can aid in the development of credible predictions of future changes. Here, we evaluate 6 available earth system models used in CMIP5 against two cross-cutting metrics, which test the models’ ability to account for changes in ocean biogeochemistry on seasonal time frames. The first metric is based on satellite-derived estimates of ocean color, focusing on NPP and NCP. The second metric is based on the seasonal cycles in atmospheric potential oxygen (APO), an atmospheric tracer that varies seasonally, mainly due to air–sea exchanges of O₂ (Stephens et al., 1998; Manning and Keeling, 2006).

EP is the ocean color-derived flux most relevant to the biological pump, but cannot be directly observed by remote sensing. It is derived by a combination of remote measurements and poorly constrained models, which inherently increases its uncertainty

8489

(Schneider et al., 2008; Nevison et al., 2012a). The quantity actually observed from space is spectral top of the atmosphere radiance, which is used to estimate chlorophyll (or another proxy of phytoplankton biomass); chlorophyll and other variables such as photosynthetic radiation are used to estimate NPP and, finally, NPP is used to estimate EP. Here, we address the commonly observed bias in standard satellite algorithms by using algorithms tuned to Southern Ocean datasets (Mitchell and Kahru, 2009) blended with more or less standard products elsewhere (Kahru and Mitchell, 2010).

Observed seasonal cycles in APO provide a new benchmark for the ocean biogeochemistry model components of ESMs. They offer evaluation metrics complementary to ocean color products by providing additional information on deep ventilation processes unavailable from satellite data alone. The main drawback of APO seasonal cycles is that atmospheric transport models (ATMs) are needed to translate ocean model air–sea O₂ fluxes into a seasonal APO signal, which inevitably introduces uncertainty (Stephens et al., 1998; Nevison et al., 2012a). A first attempt has been made to use APO seasonal cycles to evaluate ocean-only marine biogeochemistry models (Naegler et al., 2007), but the models in that study implemented a simplified parameterization of the biological processes affecting O₂ and CO₂ air–sea fluxes and were considerably less advanced than the current ecosystem dynamics and biogeochemical components used in state-of-the-art ESMs. Further, while Naegler et al. asserted that the uncertainty introduced by ATMs was too large to provide a strong constraint on ocean model fluxes, their study relied on only two ATMs. Here, we translate the model air–sea fluxes into APO signals using a wider range of ATMs and show that, in many cases, the discrepancies between modeled and observed APO seasonal cycles transcend ATM uncertainty.

8490

2 Methods

2.1 Ocean biogeochemistry models

The CMIP5 models analyzed in this study include the Geophysical Fluid Dynamics Laboratory (GFDL) Earth System Models (depth-based ESM2M and density-based ESM2G vertical oceans; Dunne et al., 2012) from Princeton, New Jersey; the Institut Pierre-Simon Laplace Coupled Model 5 in its low resolution version (IPSL-CM5A-LR, referred to as IPSL in the following) model from Paris, France; the Community Ecosystem Model (CESM) from the National Center for Atmospheric Research in Boulder; CO, the Max Planck Institut fuer Meteorologie (MPIM) Earth System Model, version MPI-ESM-LR, from Hamburg, Germany; and the Norwegian Earth System Model (NorESM1-ME, referred here as NorESM1). The ocean biogeochemical models embedded in the respective ESMs are represented by TOPAZ (GFDL) (Dunne et al., 2013), PISCES (IPSL) (Aumont and Bopp, 2006), BEC (CESM) (Moore et al., 2002, 2004, 2013), and HAMOCC (MPIM) (Ilyna et al., 2013). NorESM1 uses a variant of HAMOCC, adapted to a sigma coordinate ocean circulation model (Tjiputra et al., 2013).

The six ESMs differ in their physical components and implement ocean biogeochemical schemes that vary in their specifics, but have many common features. All include explicit representations of upper ecosystem dynamics that distinguish at least one phytoplankton group and one size class of zooplankton. Four of the models (CESM, both GFDL variants and IPSL) divide phytoplankton further into at least 2 size classes: large (micro) and small (nano + pico). GFDL and CESM also explicitly model diazotrophs. Phytoplankton growth rates in all models are co-limited by light, temperature and nutrient (N, P, Si, Fe) availability. Carbon export flux is closely linked to ecosystem structure and dynamics, with higher sinking rates assumed for large phytoplankton, representing, e.g., diatoms.

Output was obtained from the six models for the standard historical (1850–2005) prescribed atmospheric CO₂ case either directly from the individual modeling groups or through a collective web interface created for the CMIP5. The output fields included

8491

Please define
these variables

carbon export flux at 100 m depth (EP₁₀₀), vertically integrated NPP, net air–sea O₂ and CO₂ fluxes, net surface heat flux (Q), and sea surface salinity and temperature (SST). The first two fields were compared directly to the corresponding satellite ocean color products. The remaining 5 fields were used in the estimation of APO time series, with the final three fields used to estimate air–sea N₂ fluxes based on the $Q(dS/dT)_{N_2}/C_p$ equation (Keeling et al., 1993; Manizza et al., 2012) with modifications from Jin et al. (2007). The resulting N₂ fluxes, together with the prognostic O₂ and CO₂ air–sea fluxes, were used as described below to force atmospheric transport model simulations to compute atmospheric time series of APO (Naegler et al., 2007; Nevison et al., 2008, 2012a). Since all the ocean models operated on an irregular, off-polar grid with 2-dimensional latitude and longitude coordinates, these were first interpolated to a regular 1° × 1° latitude/longitude grid using Climate Data Operators freeware (<https://code.zmaw.de/projects/cdo>). The CDO interpolation was not mass conservative, but resulted in global O₂ flux differences generally of less than 1 %. An exception was CESM, whose output was converted conservatively to a regular grid using a CESM-specific mapping file.

2.2 Atmospheric transport model simulations

2.2.1 Matrix method

A matrix method was used to translate the ocean model air–sea O₂, N₂ and CO₂ fluxes into corresponding annual mean cycles in atmospheric potential oxygen (APO). The method was based on the pulse-response functions from the Transcom 3 Level 2 (T3L2) atmospheric tracer transport model (ATM) intercomparison. Each of the 13 ATMs that participated in T3L2 conducted forward simulations in which a uniformly distributed CO₂ flux pattern, normalized to 1 Pg C yr^{−1}, was released from each of 11 ocean regions for each of 12 “emission months,” i.e., January–December, allowed to decay for 35 months, and sampled every month at a range of surface monitoring sites. A map of the Transcom regions can be found at <http://transcom.project.asu>.

8492

edu/transcom03_protocol_basisMap.php. The APO code was developed from an earlier pulse-response matrix code, which has been described in detail in Nevison et al. (2012b), that translated terrestrial net ecosystem exchange (NEE) fluxes of carbon into the corresponding annual mean cycles in atmospheric CO₂. The matrix method is considerably faster than a full forward ATM simulation, allowing annual mean cycles in APO from 13 different ATMS to be computed in seconds, rather than the days or weeks required for a single forward simulation.

The pulse-response matrix code was applied separately to the O₂, N₂ and oceanic CO₂ fluxes from the last 12 years of the historical simulations, spanning 1994–2005, converting from carbon to oxygen or nitrogen units where appropriate, to create three separate time series of atmospheric O₂, N₂ and CO₂ as mole fraction anomalies (μmol mol⁻¹) on a H₂O-free basis, where the O₂ and N₂ anomalies are computed as though O₂ and N₂ were trace gases, similar to CO₂. These were combined to calculate a 9-year time series in APO in per meg units, spanning 1997–2005, according to Eq. (1):

$$\text{APO} = \frac{1}{X_{\text{O}_2}}(\text{O}_2) - \frac{1}{X_{\text{N}_2}}(\text{N}_2) + \frac{1.1}{X_{\text{CO}_2}}(\text{CO}_2) \quad (1)$$

where X_{O_2} and X_{N_2} are the total mole fractions of O₂ and N₂ in H₂O-free air, treated here as constants (0.20946 and 0.78084, respectively). The mean seasonal cycle was computed by detrending the time series with a 3rd order polynomial and then taking the average of the detrended data for all Januaries, Februaries, etc. The matrix method involves calculating separately the components of the APO time at each measurement site arising from fluxes from each ocean region. These components are then summed to compute the net APO signal. The model definition of APO in Eq. (1) ignores contributions to APO from land biospheric exchanges and fossil fuel burning, but these are very small in comparison to oceanic contributions on seasonal time scales (Manning and Keeling, 2006; Nevison et al., 2008).

8493

2.2.2 Evaluation of matrix method based on APO Transcom

An evaluation exercise was conducted in which the APO pulse-response matrix code was forced by climatological O₂ and N₂ fluxes from Garcia and Keeling (2001) and used to compute the mean seasonal cycle in APO as described above using Eq. (1) (minus the oceanic CO₂ term). The matrix-based results were evaluated against the mean seasonal cycles from archived forward ATM simulations from the APO Transcom Experiment, which also used the Garcia and Keeling O₂ and N₂ forcing fluxes (Blaine, 2005; Nevison et al., 2012b). The matrix method performed well in relatively homogeneous regions like the Southern Ocean and at northern high latitude sites like Barrow, Alaska (BRW) and Alert, Canada (ALT). It was less reliable in capturing the forward simulation cycle at sites located within Northern midlatitude ocean regions, including Cold Bay, Alaska and La Jolla, California, where the uniform distribution of fluxes assumed by T3L2 did not accurately capture the impact of strong heterogeneity in air–sea fluxes from these regions (Tables S1 and S2 and Figs. S1 and S2). These same North Pacific stations are subject to large uncertainty in full forward ATM simulations due to strong seasonal rectifier effects (Stephens et al., 1998; Battle et al., 2006; Tohjima et al., 2012). We therefore focus in Sect. 3 on ALT, BRW and several Southern Ocean sites, including Macquarie Island (MQA), Palmer Station, Antarctica (PSA) and South Pole (SPO) in our use of APO to evaluate the ESM-simulated air–sea O₂, N₂ and CO₂ fluxes.

While the evaluation exercise indicates that the matrix method reproduces the shape and phase of the seasonal cycles with high reliability at the above sites, it tends to underestimate the seasonal amplitude by about 4–5 % at ALT and BRW and by 11–12 % at MQA and SPO and to slightly overestimate the amplitude at PSA. In applying the matrix code to the ESM oceanic fluxes, we therefore scaled up the estimated cycles by site and ATM-specific scaling factors obtained from the evaluation exercise (Tables S1 and S2, Fig. S2). Since these scaling factors were only available for a subset of 9 of the original 13 T3L2 ATMs that also participated in APO Transcom, we subsequently

8494

(Sect. 3.1) compare observations alternatively to the scaled 9-model subset, or to all 13 unscaled models.

2.2.3 Component O₂ fluxes

The net air–sea O₂ flux for each ESM can be divided into three components, associated with NCP, deep ventilation and thermal processes (Nevison et al., 2012a):

$$F_{O_2, \text{total}} = F_{O_2, \text{NCP}} + F_{O_2, \text{vent}} + F_{O_2, \text{therm}} \quad (2)$$

These in turn can be used to force the matrix model and the resulting total APO cycle can be presented as the sum of component signals according to Eq. (3).

$$\text{APO} = \text{APO}_{\text{NCP}} + \text{APO}_{\text{vent}} + \text{APO}_{\text{therm}} \quad (3)$$

Here, the APO_{therm} term also includes the effects of N₂ fluxes, as per the second right-hand term in Eq. (1). The atmospheric signal due to oceanic CO₂ (last term in Eq. 1) is not easily included in any of the component terms in Eq. (3) based on available ESM output, but in principle all three component processes may lead to changes in CO₂ fluxes as well as O₂ fluxes. In practice, CO₂ has only a small influence on the amplitude and phasing of APO in most of the ESMs and thus is ignored in the component analysis. An exception is MPIM, in which the oceanic CO₂ signal has a peak-to-trough seasonal amplitude of up to 5 ppm in the Southern Ocean that opposes the O₂ cycle, as noted previously (Anav et al., 2013) and discussed further below.

Among the terms in Eq. (2), $F_{O_2, \text{total}}$ was provided outright by the ESMs and the thermal component $F_{O_2, \text{therm}}$ can be derived easily from standard ESM output following the approach described above for N₂. The remaining terms, $F_{O_2, \text{NCP}}$ and $F_{O_2, \text{vent}}$ are more challenging to estimate from available ESM output. In Nevison et al. (2012a), $F_{O_2, \text{NCP}}$ was estimated from EP multiplied by a molar ratio of 1.4 mol O₂ per mol C exported. The assumption that $F_{O_2, \text{NCP}} = 1.4 \text{ EP}$ was shown in Nevison et al. (2012a) to yield reasonable results for EP derived from satellite data (and indeed was applied to the

8495

satellite data described below in Sect. 2.3), but this approach proved unsatisfactory for EP₁₀₀ from the ESMs, especially in the Southern Ocean as discussed further below, since it yielded an atmospheric signal that was unreasonably small. The assumption also led to phasing uncertainties for some models (IPSL, NorESM1 and MPIM) that use finite sinking velocities for particulate organic carbon (as opposed to instantaneous vertical redistribution, as assumed, e.g., by CESM) with a resulting delay in EP₁₀₀ relative to NPP. Since the timing of $F_{O_2, \text{NCP}}$ is likely to be more closely related to NPP than EP₁₀₀ (Nevison et al., 2012a), we estimated $F_{O_2, \text{NCP}}$ from the ESMs alternatively as 1.4 EP₁₀₀ and 1.4 ef · NPP, where NPP is the standard, vertically-integrated ESM output variable and ef is the model-specific annual mean EP₁₀₀/NPP ratio, integrated over the 40–60° N or 40–60° S latitude band for northern and southern stations, respectively.

Finally, $F_{O_2, \text{vent}}$ in principle can be estimated as a residual of the other 3 terms in Eq. (2). $F_{O_2, \text{vent}}$ was estimated with reasonable success at the Northern Hemisphere sites, but generally looked unreasonable in the Southern Ocean for most models, with the exception of IPSL. The signals were judged to be unreasonable on the basis of whether the APO_{vent} term, if estimated as a residual from Eq. (3), dominated the APO_{NCP} term in driving the springtime rise in APO. In reality, the APO_{NCP} term must be primarily responsible for this rise (Keeling et al., 1993; Bender et al., 1996; Nevison et al., 2012a). Lacking a consistent method for estimating a reasonable $F_{O_2, \text{vent}}$ term in both hemispheres using available ESM output, we do not attempt to explicitly resolve or present APO_{vent} signals in this study.

2.3 Satellite ocean color data

The primary output product of satellite ocean color measurements historically has been the concentration of chlorophyll *a* (Chl), which is also the main input to most satellite-based ocean primary productivity models (Behrenfeld and Falkowski, 1997). However, the standard Chl product based on empirical band-ratios of reflectances represents primarily the coefficient of total absorption of blue light and is inherently biased if the distributions of the optically active components deviate from the global “mean” (Lee

8496

Please support this discussion with a supplementary figure

terms in the fit from 1 to 4 yielded a maximum that generally fell within ± 5 days of the standard 2-harmonic fit maximum, providing a measure of the uncertainty in the phase metric. The same approach was used to derive the day of the seasonal NPP maximum, except that the fit was applied to monthly mean satellite-derived and ESM NPP integrals summed from 40–60° S and 40–60° N, which were compared to the APO phase metric at southern and northern stations, respectively.

3 Results

3.1 APO comparison to Earth System Models

The APO cycles estimated from the 6 ESM air–sea fluxes were compared to observations at 3 Southern Ocean and 2 northern monitoring sites (Fig. 1). In these plots, the green envelope reflects our best estimate of the ATM uncertainty in the ocean model APO signal based on the 9 scaled ATM results, while the gray window reflects the more complete range of uncertainty using all 13 unscaled ATM results. In general, the distinction between the green and gray windows is only moderately important, as the observed APO cycle in most cases either falls within both envelopes or lies outside of both envelopes.

The MPIM and related NorESM1 ocean biogeochemistry models are examples in which the observed APO cycle lies outside both ranges of uncertainty at all 5 evaluation sites (Fig. 1, lower middle and right panels). For these models, the rise in the APO cycle occurs too early in the springtime in both hemispheres, while the overall amplitude of the cycle is too large at all the southern stations. Here, it is notable that the MPIM APO amplitude would be even larger in the Southern Ocean if it were not offset by the unrealistically large seasonal cycle in oceanic CO₂ described above. The large CO₂ cycle, however, does not substantially alter the phase of APO, which is determined mainly by the timing of the O₂ fluxes.

8499

IPSL is another ocean biogeochemistry model for which the observed APO cycle lies outside of both the best guess and full range of uncertainty at all monitoring sites, with the exception of Palmer Station (64.9° S), where observed APO falls within the wider gray window of uncertainty (Fig. 1b, lower left panels). Unlike MPIM and NorESM1, the rise in the IPSL APO cycle occurs somewhat later in the springtime than observed, while the overall amplitude of the cycle tends to be underestimated. The underestimate is mild at all the southern stations, and even falls within the broader range of uncertainty at PSA, but is more pronounced at the northern monitoring sites, where the IPSL amplitude is too small by nearly a factor of 2.

CESM is the top-performer among the 6 ESMs evaluated, consistently yielding green/gray windows that encompass the observed APO cycle at most/all of the 5 monitoring sites (Fig. 1, upper left panels). GFDL ESM2M (depth-based coordinates) is the second most consistent performer, yielding cycles that generally agree with observations, with exceptions at BRW, where ESM2M tends to mildly underestimate the depth of the APO trough, and at PSA, where the rise in the APO cycle may be up to 1 month too early. The sigma-coordinate GFDL ESM2G model is the third best performer, capturing the observed APO cycle relatively well at most southern stations, but underestimating the seasonal amplitude at the northern stations.

3.1.1 Regional analysis of APO cycle

The matrix method can partition the ocean model APO cycles into regional contributions from the 11 ocean regions used in Transcom 3L2. At the southern stations of SPO, PSA, and MQA, this partitioning reveals, not surprisingly, that the Southern Ocean (defined as all ocean regions south of 45° S) dominates the APO cycle (not shown). However, at BRW and ALT at least 3 regions make important contributions, including the “temperate” North Pacific (extending from 15° N to the Bering Strait around 65° N and thus including the subpolar region), the “temperate” North Atlantic (extending from 15° N to 48° N) and the “Northern Ocean” (including the Arctic Ocean and the North Atlantic north of 48° N). The Northern Ocean is the most important contributor

8500

to the APO seasonal cycle at both BRW (Fig. 2) and ALT and is by far the most variable component among the 6 ESMs. The largest Northern Ocean signals are seen for CESM and NorESM1, which are the only two models that reproduce the observed APO amplitude at BRW (Fig. 1d).

3.1.2 Partitioning of APO cycle among component signals

To probe further into the underestimate of the APO amplitude at BRW by most of the ESMs, we partitioned APO into thermal and NCP-related components, as described in Sect. 2.2.3 (Fig. 3). A comparison of CESM and ESM2M in Fig. 3 indicates that both have similar $\text{APO}_{\text{therm}}$ and APO_{NCP} signals, but that CESM captures total APO more or less correctly while ESM2M underestimates the total APO amplitude. By inference, the missing APO_{vent} term accounts for the difference. (As discussed in Sect. 2.2.3, APO_{vent} is not presented in Fig. 3 due to difficulties in resolving this residual term consistently across APO monitoring sites using standard ESM output). The four remaining ESMs have APO_{NCP} cycles of similar or smaller amplitude than CESM, which in the case of ESM2G and MPIM is due primarily to their relatively low ef-ratios, and all these models substantially underestimate the total APO amplitude at BRW. This suggests that these models probably also underestimate some combination of deep ventilation and NCP.

A similar partitioning of APO was attempted in the Southern Ocean, but the estimation of APO_{NCP} from model EP₁₀₀ generally did not give plausible results in this region. This problem is discussed in more detail in Sect. 4.

3.2 Satellite data compared to ESMs

Estimates of net primary production display a wide variety of spatial patterns among models and satellite data (Fig. 4). Global totals range over more than a factor of 2 (34–82 Pg C yr⁻¹) among the ESMs, with most models tending to exceed the VGPM satellite-based estimate of 45 Pg C yr⁻¹ (Table 1). Global EP is more consistent among the models, with a value around 8 Pg C yr⁻¹ in most cases, in good agreement with the

8501

satellite-based estimate. Global EP converges among the ESMs because the model with highest global NPP (ESM2M) has a small ef-ratio of <0.1 and the models with lowest global NPP (IPSL, NorESM1) have the largest ef-ratios of about 0.2 (Table 1).

The high global NPP totals in the ESMs are driven in large part by high tropical NPP values, which generally are not reflected in the satellite data except along coastlines (Fig. 4). In this paper, we focus on the 40–60° latitude bands, which are more important than the tropics in driving the seasonal cycles in NPP, EP (NCP) and APO (Garcia and Keeling, 2001; Anav et al., 2013). In the Southern Ocean 40–60° S band, global NPP ranges among ESMs from 5.2 to 12.5 Pg C yr⁻¹, encompassing the satellite-based estimates (Table 1, Fig. 5). However, the ESMs tend to underestimate EP relative to the satellite-derived values, particularly the SPGANT/Laws product, due largely to the small model ef-ratios. In the 40–60° N band, the ESMs generally underestimate both NPP and ef-ratios relative to the satellite-derived values. This combination leads to model EP values that are smaller than satellite EP by a factor of 2 on average (Table 1). In both hemispheres, the model NPP maximum tends to occur earlier than the satellite-derived maximum, with some models (IPSL, MPIM) predicting a maximum that is up to 1–2 months early (Fig. 5).

3.3 Combining APO and satellite data

3.3.1 Phase metrics

The phase metrics reveal characteristic patterns for each ESM, which are relatively consistent across APO monitoring sites. The APO seasonal maxima of MPIM and NorESM1 are earlier than observed by about 1 month and 3 weeks, respectively, on average, while the IPSL APO maximum (with the exception of PSA) tends to be later than observed by 2–3 weeks (Fig. 6). The remaining models, CESM, ESM2M and ESM2G, have seasonal APO maxima that are relatively consistent with observations, although with some variation among different stations.

8502

The observed seasonal maximum of NPP occurs about 30–40 days earlier than the observed APO maximum at the Southern Ocean stations and about 50 days earlier at BRW and ALT. Of the models, ESM2G, CESM and ESM2M capture the phase of the NPP maximum to within about 1–3 weeks, although as noted above in Fig. 5 the model NPP maxima tend to occur earlier than the satellite-based maxima. In MPIM, the NPP maximum is about 1 to 1.5 months earlier than observed, and the APO maximum is also corresponding early. IPSL is an outlier from the general slope of the APO vs. NPP phase relationship, as defined by the rest of the ESMs. The IPSL NPP maximum occurs about 40 days earlier than observed in the Southern Hemisphere and nearly 2 months earlier than observed in the Northern Hemisphere, but IPSL, curiously, also has the latest APO seasonal maximum of any of the models. NorESM1 is another outlier in the opposite direction off the general APO vs. NPP phase slope, at least in the Northern Hemisphere (Fig. 6). There, NorESM1's seasonal maximum in NPP has a relatively small lag from the APO maximum compared to the other models. NorESM1 is also unusual in that the APO_{therm} seasonal maximum at Barrow occurs about 1 month later than in any of the other ESMs (Fig. 3).

3.3.2 Seasonal amplitudes

In addition to evaluating the phasing of the ocean model APO and NPP cycles, we examined the amplitude of the cycles, with the caveat that the absolute magnitude of satellite-based NPP is not well determined and at present provides a relatively weak constraint on the models. Furthermore, the APO seasonal amplitude in principle is more closely related to NCP (or EP) than NPP. However, we chose NPP for the seasonal amplitude analysis due to the strong discrepancies in ef-ratio among models and satellite data indicated in Table 1, which may unduly bias the results.

A cross plot of the seasonal amplitude in APO against the seasonal amplitude of NPP integrated between 40–60° S suggests a strong correlation between the amplitudes of APO and NPP among the ocean biogeochemistry models, with larger NPP amplitudes associated with larger APO cycles. The strong correlation holds at all Southern Ocean

8503

stations and is illustrated in Fig. 7a at Macquarie. The cluster of top-performing ESMs (CESM, ESM2M, ESM2G) agrees relatively well with the observed APO and SPGANT amplitudes. Meanwhile both the APO and NPP amplitudes are underestimated by IPSL and overestimated by NorESM1 and MPIM.

Cross plots of the seasonal amplitudes of APO and NPP in the Northern Hemisphere reveal that these amplitudes are positively correlated at BRW (Fig. 7b) and ALT, although the correlation is weaker than in the Southern Hemisphere. CESM, ESM2G, ESM2M and MPIM all capture the satellite-based NPP seasonal amplitude relatively well, while both CESM and NorESM1 capture the observed APO amplitude. However, CESM is the only model that accurately reproduces both the NPP and APO seasonal amplitudes well relative to the observations.

4 Discussion

4.1 Northern Ocean

Most ESMs tend to underestimate substantially the observed seasonal amplitude of APO at Barrow, Alaska. A combination of region-specific results (Fig. 2) and O₂ component analysis (Fig. 3) suggests that some combination of deep ventilation and export production in the Northern Ocean (including the North Atlantic north of 48° N) in particular may be underestimated in many models. The combined analysis of the APO vs. NPP seasonal amplitudes (Fig. 7b) supports these conclusions and suggests that, while several models may be capturing primary production well in the Northern Ocean, accurate representation of export production and deep ventilation is also important for reproducing the observed APO cycle. The inference from APO that the GFDL models may have weak ventilation in the North Atlantic is not easily reconciled, however, with the finding of Dunne et al. (2012), who report robust NADW formation in both the ESM2M and ESM2G versions. Still, the stronger Atlantic overturning reported by

8504

Deep water formation may be OK, but if the biogeochemical gradients across which it acts are too weak, you could reconcile these findings.

Dunne et al. for ESM2M relative to ESM2G appears consistent with the larger APO amplitude predicted for ESM2M relative to ESM2G (Fig. 1d).

We investigated several additional mechanisms that might explain the differences among models in the APO cycle at high northern latitudes, including subpolar heat transport and Arctic sea ice cover. Here, stronger northward heat transport should lead to more deep ventilation, while lower sea ice cover will permit more production and ventilation in the Arctic Ocean. Subdividing the Northern Ocean region into Arctic Ocean and North Atlantic components revealed that some models (IPSL and ESM2G) have a very small APO seasonal amplitude component (<2 per meg) coming from the Arctic Ocean alone (Fig. 8). In ESM2G this may be related to the extensive winter sea ice cover, which exceeds the observed covered area reported by the National Snow and Ice Data Center (http://nsidc.org/data/seaice_index/archives.html) by about $2 \times 10^6 \text{ km}^2$ (Fig. 9). However, sea ice cover is lower than observed in IPSL, suggesting the small Arctic APO component in that model is more related to a general underestimate of primary and export production (e.g., as shown in Figs. 5b and 7b). While it seems clear that the strong APO seasonality in CESM can be attributed in part to its high productivity and EP in the northern subpolar and polar regions (Fig. 5 and Table 1), a full explanation for the underlying mechanisms of the CESM fidelity on APO compared to the other models is not readily apparent from surface-only data. This suggests the need for a more detailed exploration of ocean interior ventilation and biological response interactions outside the scope of the present work.

4.2 Southern Ocean

Compared to the Northern Hemisphere stations, the ESMs generally are more successful in the Southern Ocean in capturing the observed APO cycle (Fig. 1). Within the range of ATM uncertainty, at least 3 models, CESM, ESM2M, ESM2G (and IPSL at Palmer Station), predict seasonal APO amplitudes in agreement with observations. Although the Southern Ocean APO amplitude in these models varies over as much as 20 per meg, we currently are not able to distinguish which of the underlying air–sea

8505

O₂ flux fields is the most accurate, due to the uncertainty associated with translating these fluxes into an atmospheric signal. However, the APO constraint is sufficiently robust to indicate that NorESM1 and MPIM substantially overestimate some combination of production and deep ventilation in the Southern Ocean, while IPSL probably tends to underestimate these fluxes (Table 1, Fig. 7a). Reducing ATM uncertainty is a challenging problem that potentially can be addressed by using column-integrated APO signals as more aircraft data become available, or conversely, by using vertical profiles to identify top-performing ATMs (Stephens et al., 2007).

A second complication in the Southern Ocean analysis is that the EP₁₀₀ values reported by the ESMs clearly are not directly comparable to satellite NCP(EP) data, particularly our SPGANT product, and thus can not be translated readily into air–sea O₂ fluxes associated with NCP. A likely problem is that the 100 m depth horizon used to compute EP may not be comparable across satellite algorithms and ocean biogeochemistry models. EP₁₀₀ will underestimate the model's true NCP-related O₂ outgassing flux if organic matter is respired as it sinks from the actual model mixed layer depth to 100 m depth (Najjar et al., 2007). It is also puzzling that the ef-ratios predicted by the ESMs (Table 1) appear to have decreased considerably in some cases (MPIM, IPSL) relative to those reported for earlier versions of the same models (Steinacher et al., 2010). The mean global ef-ratio for the 6 ESMs in the current study is only 0.14 and, even in the Southern Ocean, is only 0.17 on average, compared to satellite-based estimates of 0.18 globally and about 0.3 at high latitudes.

In CESM the Southern Ocean summer mixed layer depths (MLDs) are generally shallower than 100m and in many regions are only around 10–40m deep (Moore et al., 2013). The shallow summer MLDs may contribute to CESM's underestimate of the ef-ratio (0.18) compared to the satellite-based estimates (0.27–0.32). The even smaller ef-ratios in the GFDL models (of less than 0.1 globally and only 0.10 to 0.13 in the Southern Ocean) are more puzzling, given that both ESM2M and ESM2G predict relatively deep summer MLDs in the Southern Ocean, which even at their minimum are often deeper than 100m (Dunne et al., 2012). The small GFDL ef-ratios may be related

to an overvigorous picophytoplankton component wherein a prochlorococcus-like form is capable of competing relatively well even in cold polar waters. Small picophytoplankton are more likely to be reoxidized and remineralized within the mixed layer, whereas larger, heavier microphytoplankton (e.g., diatoms) are more likely to be exported out of the oceanic mixed layer (Uitz et al., 2010).

4.3 Phase relationships

While much of our analysis focuses on the seasonal amplitude of APO and NPP at mid to high latitudes, both of these metrics involve relatively large uncertainty. This derives from ATM uncertainty in the case of APO, while for NPP the uncertainty results from the lack of strong constraints on the absolute magnitude of the satellite fluxes. In contrast, we have relatively high confidence in the phasing of model APO, as represented by the matrix method (see Supplement) and in NPP observationally derived from satellite data, based on the close correspondence in phasing between the SPGANT and VGPM algorithms. For these reasons, we used a phase metric, i.e., the timing of the seasonal maximum, to examine relationships between observed and model APO and NPP. As in the seasonal amplitude analysis, MPIM, NorESM1, and IPSL displayed phasing patterns that tended to deviate from observations and the other three top-performing models, albeit in diverging ways. A complete diagnosis of the model physics responsible for the phasing anomalies (e.g., IPSL's early NPP maxima and late APO maxima) described in Sect. 3.3.1 is beyond the scope of this paper. Here we note mainly that the phase metrics are a robust and relatively good indicator of overall model performance with respect to APO.

5 Conclusions

We have used measurements of the seasonal cycles in APO to challenge and test the ocean model components of 6 ESMs. The model/data comparison reveals that half of

8507

the ESMs tested reproduce the observed cycles reasonably well, within the range of ATM uncertainty, while half do not. ESM performance in general is more favorable in the Southern Hemisphere than in the Northern Hemisphere, where most models appear to underestimate the wintertime ventilation of O_2 -depleted deepwater that drives the declining branch of the APO seasonal cycle and many may also underestimate both primary and export production, particularly at high northern latitudes. We used NPP and NCP(EP) products derived from satellite ocean color data as complementary constraints on the models in an effort to tighten the APO constraint, which reflects a combination of production and ventilation processes. However, while the satellite data provide relatively strong constraints with respect to phasing, they are more uncertain with respect to the absolute magnitudes of NPP and NCP(EP).

APOvent issue also seems important, as is the issue of matrix transport not doing well at lower latitudes.

At least two primary uncertainties limit our ability to place stronger constraints on ocean model biogeochemistry based on currently available information from APO and satellite data: (1) The relatively large ATM uncertainty involved in translating air–sea O_2 fluxes into APO signals. (2) The uncertainty in how model EP_{100} relates to the true model $F_{O_2, NCP}$ flux and how this relationship varies among models and satellite algorithms. The first of these, ATM uncertainty, is substantial but probably also has been overstated in previous analyses (e.g., Naegler et al., 2007). We have shown that half of the 6 ESMs tested here produce APO cycles whose mismatch with observed APO clearly transcends ATM uncertainty, suggesting underlying deficiencies in those models' physics and biogeochemistry.

Improving the understanding of the relationship between model air–sea O_2 fluxes and quantities like NPP, NCP and EP is a more tractable problem that can be dissected with appropriate model diagnostics, e.g., as per Manizza et al. (2012). Extending model-derived insights to satellite products may be more challenging and will likely require a shift in emphasis from EP at an arbitrary reference depth to near-surface processes like NCP, which are more relevant for exchanges of O_2 and CO_2 at the air–sea interface and more directly related to upward radiances detected by satellites.

Acknowledgements. The authors gratefully acknowledge the CMIP5 ocean modelers for providing the output that made this project possible. In particular, we thank Keith Lindsay, Laure Resplandy, and Cristoph Heinze for their assistance. We also thank Michael Bender and Robert Mika for providing APO data. We acknowledge support from NASA Ocean Biology and Biogeochemistry grant NNX11AL73G.

References

- Anav, A., Friedlingstein, P., Kidston, M., Bopp, L., Ciais, P., Cox, P., Jones, C., Jung, M., Myrneni, R. and Zhu, Z.: Evaluating the land and ocean components of the global carbon cycle in the CMIP5 Earth System Models, *J. Climate*, 26, 6801–6843, 2013.
- Arora, V. K., Boer, G. J., Friedlingstein, P., Eby, M., Jones, C., Christian, J., Bonan, G., Bopp, L., Brovkin, V., Cadule, P., Hajima, T., Ilyina, T., Lindsay, K., Tjiputra, J. and Wu, T.: Carbon-concentration and carbon-climate feedbacks in CMIP5 Earth System Models, *J. Climate*, 26, 5289–5314, 2013.
- Aumont, O. and Bopp, L.: Globalizing results from ocean in situ iron fertilization studies, *Global Biogeochem. Cy.*, 20, GB2017, doi:10.1029/2005GB002591, 2006.
- Aumont, O., Maier-Reimer, E., Blain, S., and Monfray, P.: An ecosystem model of the global ocean including Fe, Si, P colimitations, *Global Biogeochem. Cy.*, 17, 1060, doi:10.1029/2001GB001745, 2003.
- Battle, M., Mikaloff Fletcher, S., Bender, M. L., Keeling, R. F., Manning, A., Gruber, N., Tans, P., Hendricks, M., Ho, D., Simonds, C., Mika, R. and Paplawsky, B.: Atmospheric potential oxygen: new observations and their implications for some atmospheric and oceanic models, *Global Biogeochem. Cy.*, 20, GB1010, doi:10.1029/2005GB002534, 2006.
- Behrenfeld, M. J. and Falkowski, P. G.: Photosynthetic rates derived from satellite based chlorophyll concentration, *Limnol. Oceanogr.*, 42, 1–20, 1997.
- Bender, M., Ho, D., Hendricks, M. B., Mika, R., Battle, M. O., Tans, P., Conway, T. J., Sturtevant, P. B., and Cassar, N.: Atmospheric O_2/N_2 changes, 1993–2002: implications for the partitioning of fossil fuel CO_2 sequestration, *Global Biogeochem. Cy.*, 19, GB4017, doi:10.1029/2004GB002410, 2005.
- Blaine, T., W.: Continuous Measurements of Atmospheric Ar/N_2 as a Tracer of Air–Sea Heat Flux: Models, Methods, and Data, University of California, San Diego, La Jolla, 2005.
- Bopp, L., Resplandy, L., Orr, J. C., Doney, S. C., Dunne, J. P., Gehlen, M., Halloran, P., Heinze, C., Ilyina, T., Séférian, R., Tjiputra, J., and Vichi, M.: Multiple stressors of ocean ecosystems in the 21st century: projections with CMIP5 models, *Biogeosciences*, 10, 6225–6245, doi:10.5194/bg-10-6225-2013, 2013.
- Boyd, P. W., Doney, S. C.: The impact of climate change and feedback processes on the ocean carbon cycle, in: *Ocean Biogeochemistry, The Role of the Ocean Carbon Cycle in Global Change*, chap. 7, edited by: Fasham, M. J. R., Springer-Verlag, 157–198, 2003.
- Cadule, P., Friedlingstein, P., Bopp, L., Sitch, S., Jones, C. D., Ciais, P., Piao, S. L., and Peylin, P.: Benchmarking coupled climate-carbon models against long-term atmospheric CO_2 measurements, *Global Biogeochem. Cy.*, 24, GB2016, doi:10.1029/2009GB003556, 2010.
- Dunne, J. P., Armstrong, R. A., Gnanadesikan, A., and Sarmiento, J. L.: Empirical and mechanistic models for the particle export ratio, *Global Biogeochem. Cy.*, 19, GB4026, doi:10.1029/2004GB002390, 2005.
- Dunne, J. P., John, J., Adcroft, A., Griffies, S., Hallberg, R., Shevliakova, E., Stouffer, R., Cooke, W., Dunne, K., Harrison, M., Krasting, J., Malyshev, S., Milly, P., Phillips, P., Sentman, L., Samuels, B., Spelman, M., Winton, M., Wittenberg, A. and Zadeh, N.: GFDL's ESM2 global coupled climate-carbon Earth System Models Part I: physical formulation and baseline simulation characteristics, *J. Climate*, doi:10.1175/JCLI-D-11-00560.1, 2012.
- Dunne, J. P., John, J., Shevliakova, E., Stouffer, R., Krasting, J., Malyshev, S., Milly, P., Sentman, L., Adcroft, A., Cooke, W., Dunne, K., Griffies, S., Hallberg, R., Harrison, M., Levy, H., Wittenberg, A., Phillips, P. and Zadeh, N.: GFDL's ESM2 global coupled climate-carbon Earth System Models Part II: carbon system formulation and baseline simulation characteristics, *J. Climate*, doi:10.1175/JCLI-D-12-00150.1, 2013.
- Gruber, N. and Sarmiento, J. L.: Large-scale biogeochemical-physical interactions in elemental cycles, in: *The Sea*, vol. 12, edited by: Robinson, A. R., McCarthy, J. J., and Rothschild, B. J., John Wiley & Sons, Inc., New York, 2002.
- Henson, S. A., Sarmiento, J. L., Dunne, J. P., Bopp, L., Lima, I., Doney, S. C., John, J., and Beaulieu, C.: Detection of anthropogenic climate change in satellite records of ocean chlorophyll and productivity, *Biogeosciences*, 7, 621–640, doi:10.5194/bg-7-621-2010, 2010.

- Henson, S. A., Sanders, R., Madsen, E., Morris, P. J., Le Moigne, F., and Quartly, G. D.: A reduced estimate of the strength of the ocean's biological carbon pump, *Geophys. Res. Lett.*, 38, L04606, doi:10.1029/2011GL046735, 2011.
- Henson, S., Cole, H., Beaulieu, C., and Yool, A.: The impact of global warming on seasonality of ocean primary production, *Biogeosciences*, 10, 4357–4369, doi:10.5194/bg-10-4357-2013, 2013.
- Ilyina, T., Six, K. D., Segschneider, J., Maier-Reimer, E., Li, H., and Nuñez-Riboni, I.: Global ocean biogeochemistry model HAMOCC: model architecture and performance as component of the MPI-Earth system model in different CMIP5 experimental realizations, *J. Adv. Model. Earth Syst.*, 5, 287–315, doi:10.1029/2012MS000178, 2013.
- Irwin, A. J. and Oliver, M. J.: Are ocean deserts getting larger?, *Geophys. Res. Lett.*, 36, L18609, doi:10.1029/2009GL039883, 2009.
- Jiang, C. L., Gille, S. T., Sprintall, J., and Sweeney, C.: Drake passage oceanic $p\text{CO}_2$: evaluating CMIP5 coupled carbon–climate models using in situ observations, *J. Climate*, 27, 76–100, 2014.
- Jin, X., Najjar, R. G., Louanchi, F., and Doney, S. C.: A modeling study of the seasonal oxygen budget of the global ocean, *J. Geophys. Res.*, 112, C05017, doi:10.1029/2006JC003731, 2007.
- Kahru, M. and Mitchell, B. G.: Blending of ocean colour algorithms applied to the Southern Ocean, *Remote Sens. Lett.*, 1, 119–124, doi:10.1080/01431160903547940, 2010.
- Kahru, M., Kudela, R., Manzano-Sarabia, M., and Mitchell, B. G.: Trends in primary production in the California Current detected with satellite data, *J. Geophys. Res.*, 114, C02004, doi:10.1029/2008JC004979, 2009.
- Keeling, R. F., Najjar, R. P., Bender, M. L., and Tans, P. P.: What atmospheric oxygen measurements can tell us about the global carbon cycle, *Global Biogeochem. Cy.*, 7, 37–67, 1993.
- Keeling, R. F., Stephens, B. B., Najjar, R. G., Doney, S. C., Archer, D., and Heimann, M.: Seasonal variations in the atmospheric O_2/N_2 ration in relation to the kinetics of air–sea gas exchange, *Global Biogeochem. Cy.*, 12, 141–163, 1998.
- Keeling R. F., Koertzing, A., and Gruber, N.: Ocean deoxygenation in warming world, *Annu. Mar. Rev. Sci.*, 2, 463–493, 2010.
- Khatiwal, S., Primeau, F., and Hall, T.: Reconstruction of the history of anthropogenic CO_2 concentrations in the ocean, *Nature*, 462, 346–350, 2009.

8511

- Laws, E. A.: Export flux and stability as regulators of community composition in pelagic marine biological communities: implications for regime shifts, *Prog. Oceanogr.*, 60, 343–353, 2004.
- Laws, E. A., Falkowski, P. G., Smith Jr., W. O., Ducklow, H. W., and McCarthy, J. J.: Temperature effects on export production in the open ocean, *Global Biogeochem. Cy.*, 14, 1231–1246, 2000.
- Lee, Z., Lance, V., Shang, S., Vaillancourt, R., Freeman, S., Lubac, B., Hargreaves, B., Del Castillo, C., Miller, R., Twardowski, M. and Wei, G.: An assessment of optical properties and primary production derived from remote sensing in the Southern Ocean (SO GasEx), *J. Geophys. Res.*, 116, C00F03, doi:10.1029/2010JC006747, 2011.
- Le Quéré, C., Roedenbeck, C., Buitenhuis E. T., Conway, T. J., Langenfelds, R., Gomez, A., Labuschagne, C., Ramonet, M., Nakazawa, T., Metzl, N., Gillett, N. and Heimann, M.: Saturation of the Southern Ocean CO_2 sink due to recent climate change, *Science*, 316, 1735–1738, 2007.
- Maier-Reimer, E., Kriest, I., Segschneider, J., and Wetzel, P.: The Hamburg Ocean Carbon Cycle model HAMOCC5.1, *Berichte zur Erdsystemforschung* 14/2005, Max Planck-Institut für Meteorologie, Hamburg, Germany, 2005.
- Manizza, M., Keeling, R. F., and Nevison, C. D.: On the processes controlling the seasonal cycles of the air–sea fluxes of O_2 and N_2O : a modeling study, *Tellus B*, 64, 18429, doi:10.3402/tellusb.v64i0.18429, 2012.
- Manning, A. C. and Keeling, R. F.: Global oceanic and land biotic carbon sinks from the Scripps atmospheric oxygen flask sampling network, *Tellus B*, 58, 95–116, 2006.
- Mitchell, B. G.: Predictive bio-optical relationships for polar oceans and marginal ice zones, *J. Marine Syst.*, 3, 91–105, 1992.
- Mitchell, B. G. and Kahru, M.: Bio-optical algorithms for ADEOS-2 GLI, *J. Remote Sens. Soc. Jpn.*, 29, 80–85, 2009.
- Moore, J. K., Doney, S. C., Kleypas, J. C., Glover, D. M., and Fung, I. Y.: An intermediate complexity marine ecosystem model for the global domain, *Deep-Sea Res. Pt. II*, 49, 403–462, 2002.
- Moore, J. K., Doney, S. C., and Lindsay, K.: Upper ocean ecosystem dynamics and iron cycling in a global 3-D model, *Global Biogeochem. Cy.*, 18, GB4028, doi:10.1029/2004GB002220, 2004.
- Moore, J., Lindsay, K., Doney, S., Long, M., and Misumi, K.: Marine ecosystem dynamics and biogeochemical cycling in the Community Earth System Model (CESM1(BGC)): comparison

8512

- of the 1990s with the 2090s under the RCP4.5 and RCP8.5 scenarios, *J. Climate*, 26, 9291–9312, doi:10.1175/JCLI-D-12-00566.1, 2013.
- Naegler, T., Ciais, P., Orr, J., Aumont, O., and Roedenbeck, C.: On evaluating ocean models with atmospheric potential oxygen, *Tellus B*, 59, 138–156, 2007.
- 5 Najjar, R. G., Jin, X., Louanchi, F., Aumont, O., Caldeira, K., Doney, S., Dutay, J. C., Follows, M., Gruber, N., Joos, F., Lindsay, K., Maier-Reimer, E., Matear, R., Matsumoto, K., Monfray, P., Mouchet, A., Orr, J., Plattner, G. K., Sarmiento, J., Schlitzer, R., Slater, R., Weirig, M.-F., Yamanaka, Y. and Yool, A.: Impact of circulation on export production, dissolved organic matter, and dissolved oxygen in the ocean: results from phase II of the Ocean Carbon-cycle Model Intercomparison Project (OCMIP-2), *Global Biogeochem. Cy.*, 21, GB3007, doi:10.12007, 10 2007.
- Nevison, C. D., Keeling, R. F., Weiss, R. F., Popp, B. N., Jin, X., Fraser, P. J., Porter, L. W., and Hess, P. G.: Southern Ocean ventilation inferred from seasonal cycles of atmospheric N_2O and O_2/N_2 at Cape Grim, Tasmania, *Tellus B*, 57, 218–229, 2005.
- 15 Nevison, C. D., Mahowald, N. M., Doney, S. C., Lima, I. D., and Cassar, N.: Impact of variable air-sea O_2 and CO_2 fluxes on atmospheric potential oxygen (APO) and land-ocean carbon sink partitioning, *Biogeosciences*, 5, 875–889, doi:10.5194/bg-5-875-2008, 2008.
- Nevison, C. D., Dlugokencky, E., Dutton, G., Elkins, J. W., Fraser, P., Hall, B., Krummel, P. B., Langenfelds, R. L., O'Doherty, S., Prinn, R. G., Steele, L. P., and Weiss, R. F.: Exploring causes of interannual variability in the seasonal cycles of tropospheric nitrous oxide, *Atmos. Chem. Phys.*, 11, 3713–3730, doi:10.5194/acp-11-3713-2011, 2011.
- 20 Nevison, C. D., Keeling, R. F., Kahru, M., Manizza, M., Mitchell, B. G., and Cassar, N.: Estimating net community production in the Southern Ocean based on atmospheric potential oxygen and satellite ocean color data, *Global Biogeochem. Cy.*, 26, GB1020, doi:10.1029/2011GB004040, 2012a.
- 25 Nevison, C. D., Baker, D. F., and Gurney, K. R.: A methodology for estimating seasonal cycles of atmospheric CO_2 resulting from terrestrial net ecosystem exchange (NEE) fluxes using the Transcom T3L2 pulse-response functions, *Geosci. Model Dev. Discuss.*, 5, 2789–2809, doi:10.5194/gmdd-5-2789-2012, 2012b.
- 30 Polovina, J. J., Howell, E. A., and Abecassis, M.: Ocean's least productive waters are expanding, *Geophys. Res. Lett.*, 35, L03618, doi:10.1029/2007GL031745, 2008.
- Roy, T., Bopp, L., Gehlen, M., Schneider, B., Cadule, P., Frölicher, T., Segschneider, J., Tjiputra, J., Heinze, C. and Joos, F.: Regional impacts of climate change and atmospheric

8513

- CO_2 on future ocean carbon uptake: a multimodel linear feedback analysis, *J. Climate*, 24, 2300–2318, 2011.
- Sauer, M. J., Roesler, C. S., Werdell, J. P., and Barnard, A.: Under the hood of satellite empirical chlorophyll algorithms: revealing the dependencies of maximum band ratio algorithms on inherent optical properties, *Opt. Express*, 20, 20920–20933, 2012.
- 5 Schneider, B., Bopp, L., Gehlen, M., Segschneider, J., Frölicher, T. L., Cadule, P., Friedlingstein, P., Doney, S. C., Behrenfeld, M. J., and Joos, F.: Climate-induced interannual variability of marine primary and export production in three global coupled climate carbon cycle models, *Biogeosciences*, 5, 597–614, doi:10.5194/bg-5-597-2008, 2008.
- 10 Siegel, D. A., Maritorena, S., Nelson, N. B., and Behrenfeld, M. J.: Independence and interdependencies among global ocean color properties: reassessing the bio-optical assumption, *Geophys. Res. J.*, 110, C07011, doi:10.1029/2004JC002527, 2005.
- Sigman, D. M., Hain, M. P., and Haug, G. H.: The polar ocean and glacial cycles in atmospheric CO_2 , *Nature*, 466, 47–55, 2010.
- 15 Six, K. and Maier-Reimer, E.: Effects of plankton dynamics on seasonal carbon fluxes in an ocean general circulation model, *Global Biogeochem Cy.*, 10, 559–583, 1996.
- Steinacher, M., Joos, F., Frölicher, T. L., Bopp, L., Cadule, P., Cocco, V., Doney, S. C., Gehlen, M., Lindsay, K., Moore, J. K., Schneider, B., and Segschneider, J.: Projected 21st century decrease in marine productivity: a multi-model analysis, *Biogeosciences*, 7, 979–1005, doi:10.5194/bg-7-979-2010, 2010.
- 20 Stephens, B. B., Keeling, R. F., Heimann, M., Six, K. D., Murnane, R., and Caldeira, K.: Testing global ocean carbon cycle models using measurements of atmospheric O_2 and CO_2 concentration, *Global Biogeochem. Cy.*, 12, 213–230, 1998.
- Stephens, B. B., Gurney, K. R., Tans, P., Sweeney, C., Peters, W., Bruhwiler, L., Ciais, P., Ramonet, M., Bousquet, P., Nakazawa, T., Aoki, S., Machida, T., Inoue, G., Vinnichenko, N., Lloyd, J., Jordan, A., Heimann, M., Shibistova, O., Langenfelds, R., Steele, L., Francey, R. and Denning, A. S.: Weak northern and strong tropical land carbon uptake from vertical profiles of atmospheric CO_2 , *Science*, 316, 1732–1735, doi:10.1126/science.1137004, 2007.
- 25 Tjiputra, J. F., Roelandt, C., Bentsen, M., Lawrence, D. M., Lorentzen, T., Schwinger, J., Seland, Ø., and Heinze, C.: Evaluation of the carbon cycle components in the Norwegian Earth System Model (NorESM), *Geosci. Model Dev.*, 6, 301–325, doi:10.5194/gmd-6-301-2013, 2013.
- 30

8514

- Tohjima, Y., Minejima, C., Mukai, H., Machida, T., Yamagishi, H., and Nojiri, Y.: Analysis of seasonality and annual mean distribution of atmospheric potential oxygen (APO) in the Pacific region, *Global Biogeochem. Cy.*, 26, GB004110, doi:10.1029/2011GB004110, 2012.
- Uitz, J., Claustre, H., Gentili, B., and Stramski, D.: Phytoplankton class-specific primary production in the world's oceans: seasonal and interannual variability from satellite observations, *Global Biogeochem. Cy.*, 24, GB3016, doi:10.1029/2009GB003680, 2010.
- Vancoppenolle, M., Bopp, L., Madec, G., Dunne, J., Ilyina, T., Halloran, P. R., and Steiner, N.: Future Arctic Ocean primary productivity from CMIP5 simulations: uncertain outcome, but consistent mechanisms, *Global Biogeochem. Cy.*, 27, 605–619, doi:10.1002/gbc.20055, 2013.

8515

Table 1. Vertically integrated NPP, EP at 100 m (both in Pg C yr^{-1}) and EP/PP (ef-ratio) for 6 CMIP5 models and 2 Satellite Products.

Model	CESM	ESM2M	ESM2G	IPSL	NorESM1	MPIM	VGPM	SPGANT ^a
Global								
EP	7.97	7.78	5.27	7.02	8.00	8.26	8.20	N/A
NPP	56.3	82.2	66.5	33.6	41.0	57.9	45.42	N/A
EP/NPP	0.14	0.095	0.08	0.21	0.20	0.14	0.18	N/A
40–60° N								
EP	0.71	0.83	0.53	0.75	0.66	0.51	1.47	N/A
NPP	3.85	4.71	3.92	2.42	3.45	3.77	4.97	N/A
EP/NPP	0.19	0.18	0.14	0.31	0.19	0.13	0.30	N/A
60–90° N								
EP	0.34	0.33	0.21	0.19	0.15	0.08	0.46	N/A
NPP	1.48	1.35	0.95	0.58	0.74	0.75	1.29	N/A
EP/NPP	0.23	0.24	0.22	0.33	0.20	0.11	0.36	N/A
40–60° S								
EP	1.25	1.18	0.82	1.42	1.93	1.77	1.60	2.85
NPP	6.77	9.36	8.53	5.24	10.3	12.5	6.01	8.81
EP/NPP	0.18	0.13	0.10	0.27	0.19	0.14	0.27	0.32

^a SPGANT totals are only shown for the 40–60° S band because the algorithm is optimized for the Southern Ocean but not well validated in the Northern Hemisphere.

8516

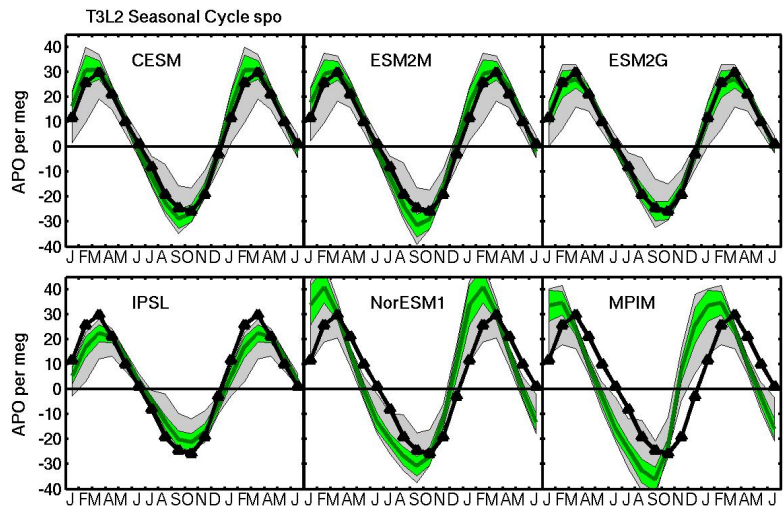


Figure 1a. Results of the pulse-response code forced by O_2 , N_2 and CO_2 air–sea fluxes from 6 ESM ocean biogeochemistry model components. The dark green line and light green window show the mean and standard deviation, respectively, of the 9 ATMs participating in both T3L2 and APO Transcom. The amplitudes are scaled for each ATM and monitoring site based on the validation exercise described in the Supplement. The gray window shows the full range of responses from all 13 T3L2 ATMs, uncorrected based on the APO Transcom validation exercise. They heavy black line shows the observed APO mean annual cycle. **(a)** Results at South Pole.

8517

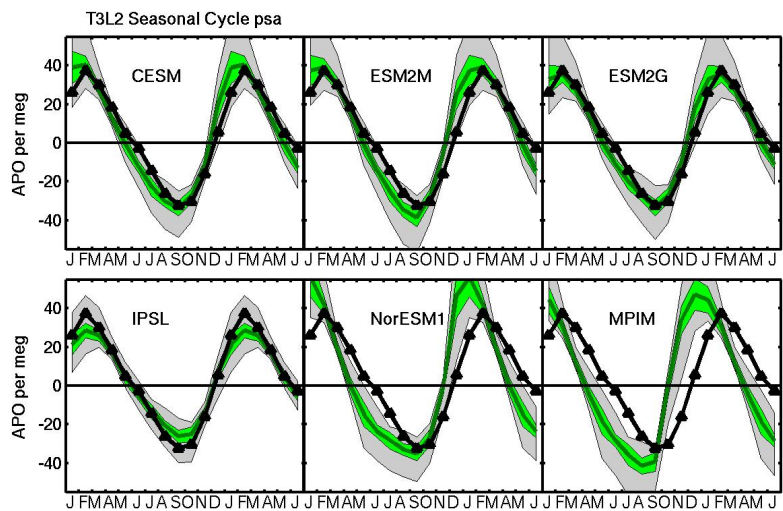


Figure 1b. Results at Palmer Station (64.9° S, 64° W).

8518

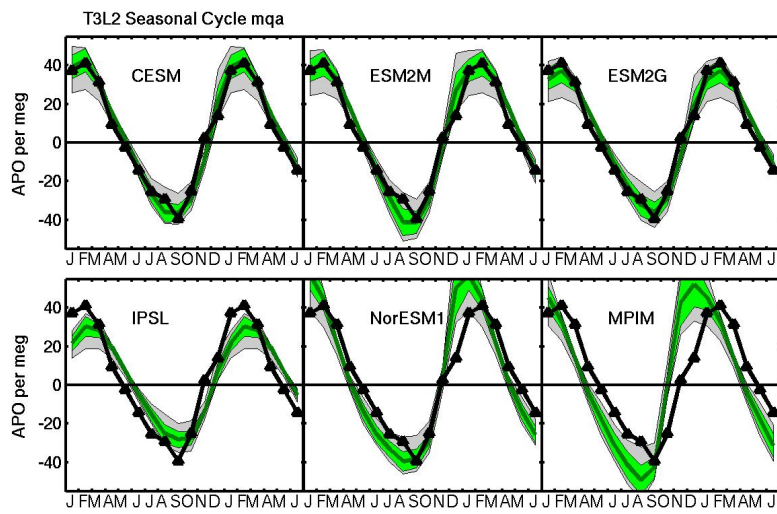


Figure 1c. Results at Macquarie Island (54.5° S, 159° E).

8519

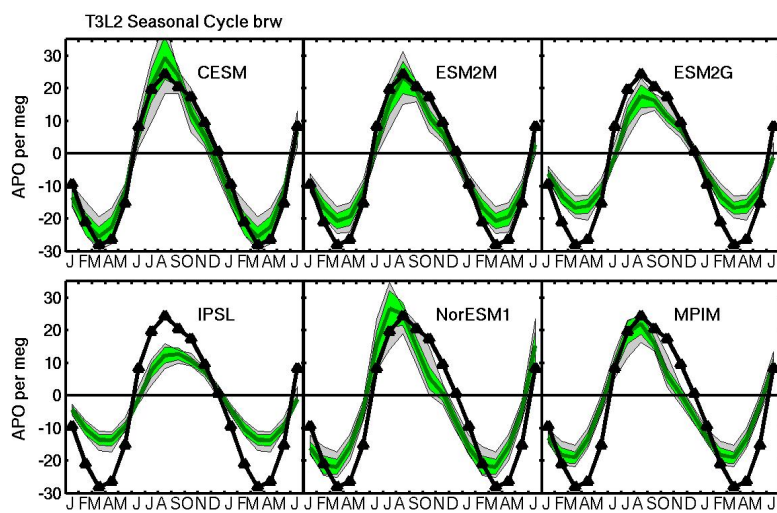


Figure 1d. Results at Barrow, Alaska (71.3° N, 156.6° W).

8520

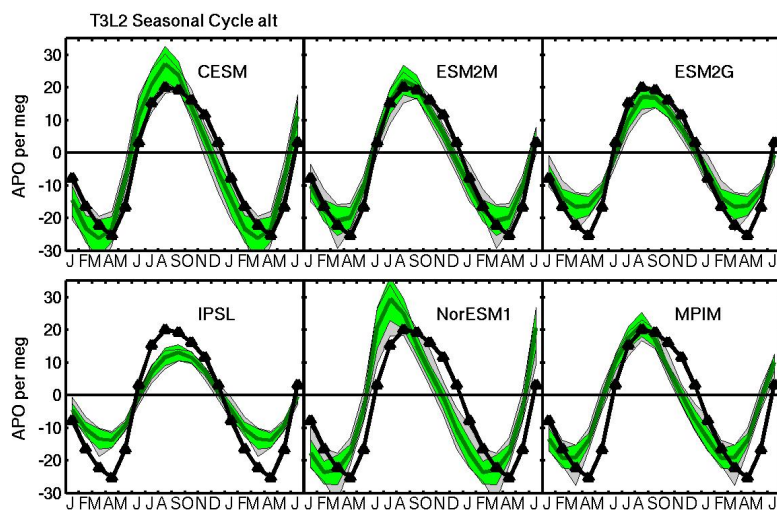


Figure 1e. Results at Alert, Canada (82.5° N, 62.5° W).

8521

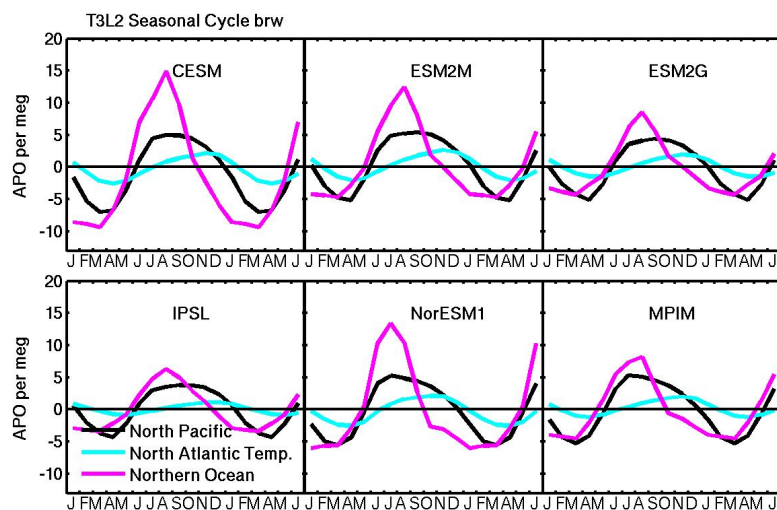


Figure 2. Partitioning APO cycle at Barrow, Alaska into main regional contributions, North Pacific (black), Temperate North Atlantic (cyan) and Northern Ocean (magenta), which includes the North Atlantic north of 48° N and the Arctic Ocean. All curves reflect unscaled model mean of 13 ATMs used in the matrix method.

8522

Include APOvent as residual

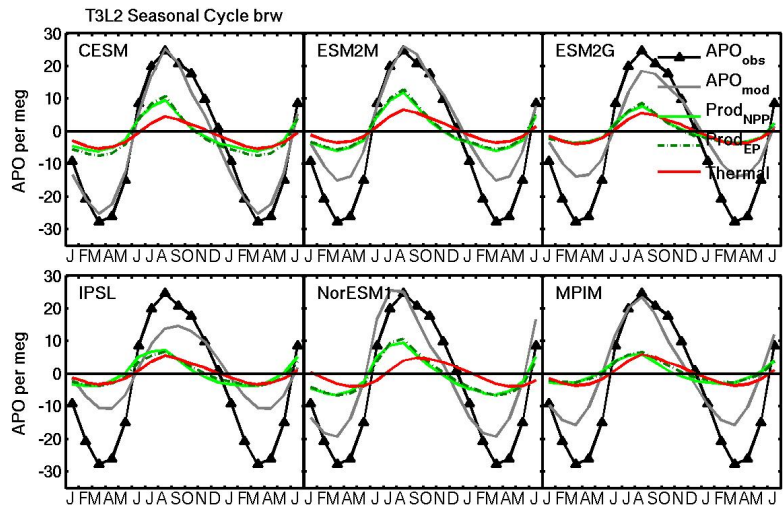


Figure 3. Partitioning of model mean APO cycle into NCP and thermal components at Barrow, Alaska. The APO_{NCP} components are estimated alternatively based on ocean model EP at 100 m (Prod_{EP} light green, solid curve) and vertically-integrated NPP (Prod_{NPP} scaled by the mean ratio of $\text{EP}_{100}/\text{NPP}$ (f ratio) between 40–60° N of the given ocean model (dark green, dashed curve). All components have been translated into atmospheric signals as described in Sect. 2.2.3. With the exception of observed APO, all curves reflect the unscaled mean of the 13 ATMs used in the matrix method.

8523

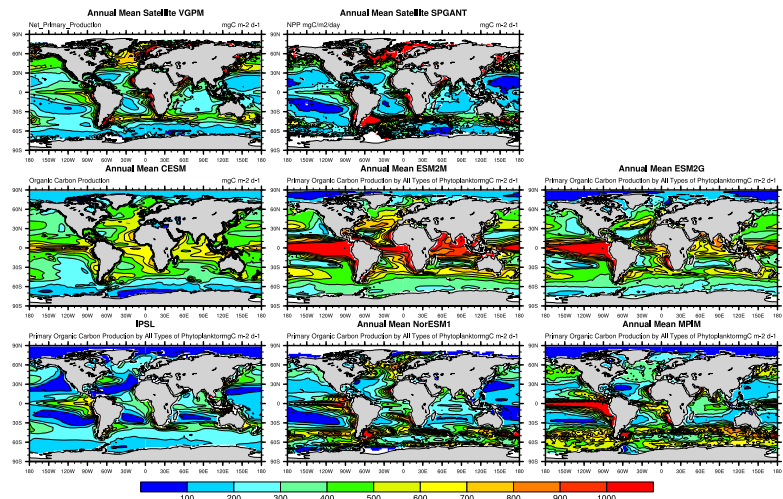


Figure 4. Annual mean NPP (in $\text{mg C m}^{-2} \text{ day}^{-1}$) using top row) MODIS-Aqua data input to the VGPM NPP model and (b) SeaWiFS data input to the SPGANT algorithm. Rows 2 and 3 show the corresponding NPP fields from 6 ESMs for the mean of 1997–2005.

Please include TRANSCOM
region boundaries in one frame
for the readers' reference

8524

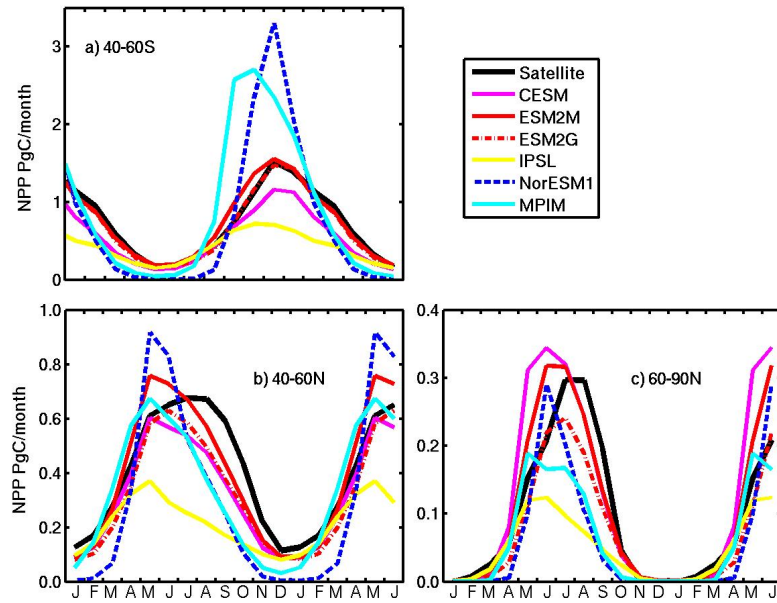


Figure 5. Comparison of NPP (PgC month^{-1}) mean annual cycle as simulated by ESMs and satellite-derived observations integrated over: **(a)** 40–60° S, **(b)** 40–60° N, **(c)** 60–90° N.

8525

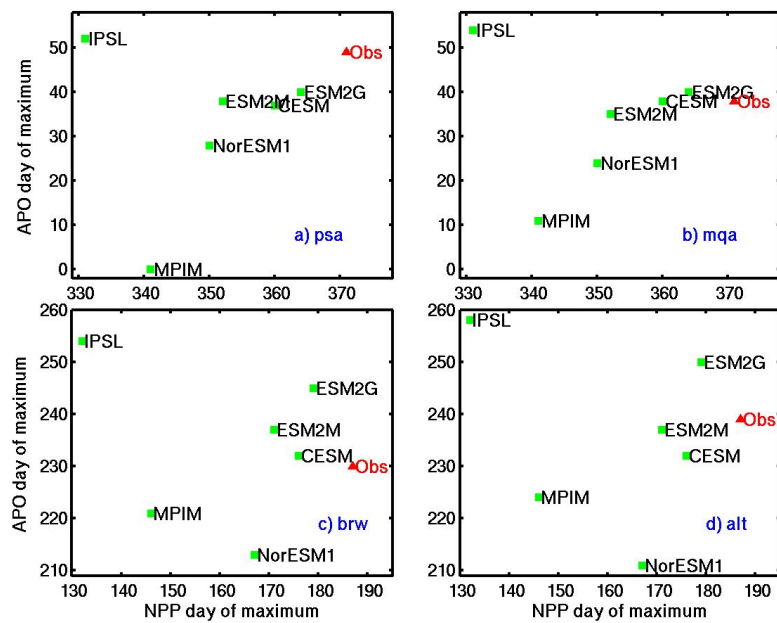


Figure 6. Day of maximum of total APO total plotted against day of maximum of NPP. The observed data point is derived from APO data at **(a)** Palmer Station, **(b)** Macquarie, **(c)** Barrow and **(d)** Alert plotted against satellite NPP data integrated over the 40–60° latitude band of the appropriate hemisphere.

8526

The labels on the y-axis should be identical

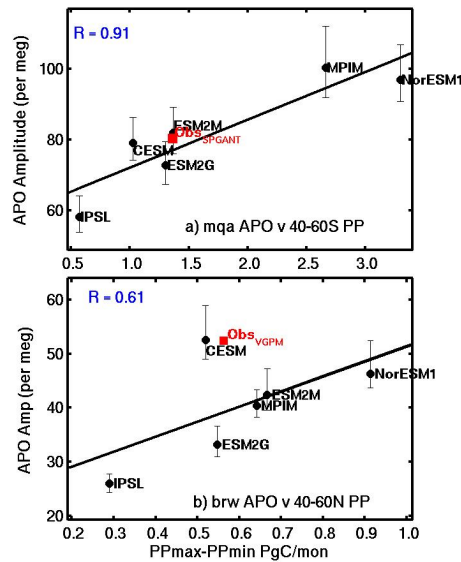


Figure 7. (a) Seasonal amplitude in APO at Macquarie Island (MQA), located at 54.5° S, 159° E, as estimated from the air–sea O_2 , CO_2 and heat fluxes from 6 ESMs, plotted against the seasonal amplitude of model NPP integrated from 40–60° S. Error bars represent the ATM uncertainty in model APO as estimated with the matrix method. The “Observed” data points (in red) are based on APO data from the Princeton network at Macquarie and NPP from the SPGANT satellite ocean color algorithm, as described in the text. Correlation slope refers to regression through ESM points only, **(b)** Same as **(a)**, but plotting seasonal amplitude in APO at Barrow, Alaska against the seasonal amplitude of model NPP integrated from 40–60° N. The “Observed” data point is based on APO data from the SIO network and the VGPM algorithm with MODIS-Aqua input.

8527

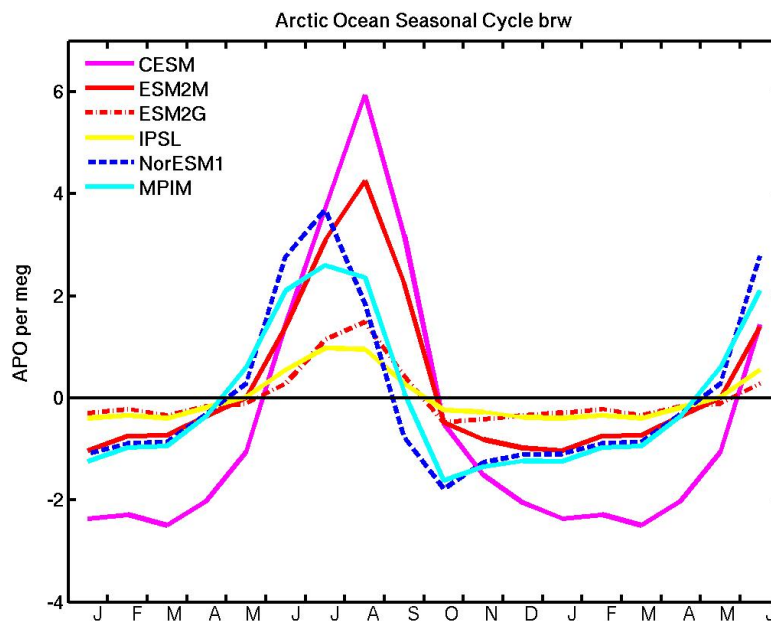


Figure 8. APO cycle at Barrow, Alaska from the Transcom Northern Ocean region, restricted to latitudes north of 65° N to estimate the contribution of the Arctic Ocean. All curves reflect the unscaled model mean of 13 ATMs used in the matrix method.

8528

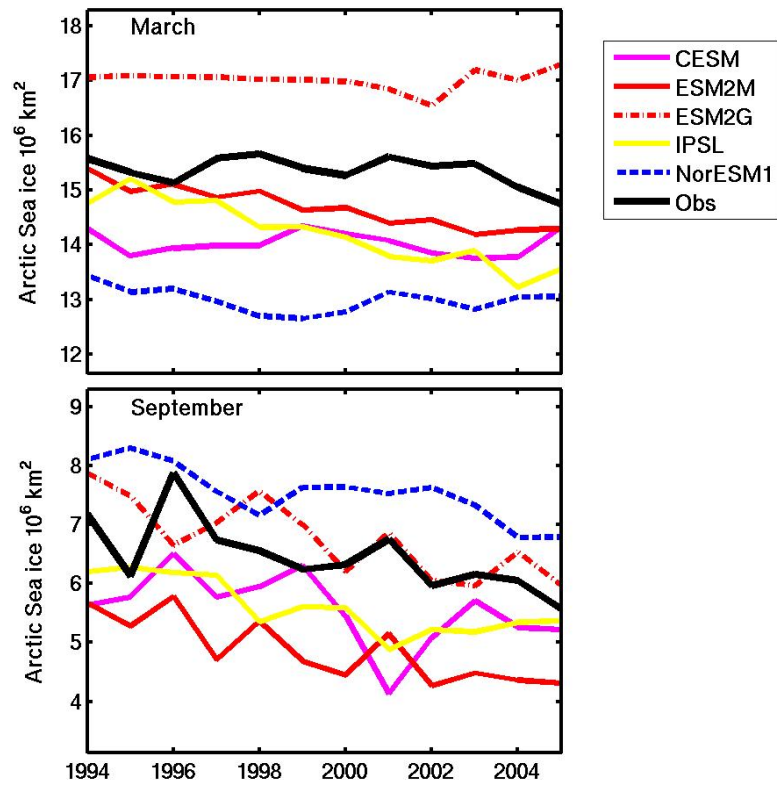


Figure 9. Changes in total Arctic sea ice cover in 10^6 km^2 predicted over 1994–2005 compared to observed values from the National Snow and Ice Data Center (MPIM seaice cover was not available for this analysis). **(a)** March, **(b)** September.